Review
Nuclear Medicine Review 2025, 28, 118–127
DOI: 10.5603/nmr.107884

ISSN 1506–9680, e-ISSN 1644–4345

VIA MEDICA

Quantification methods for ^{99m}Tc-labelled disphosphonates uptake in cardiac amyloidosis

José Manuel Belo Ferreira[1], Matilde Sousa Neves[1], Sérgio Rafael Reis Figueiredo[1, 2]

[1]Lisbon School of Health Technology, Lisbon Polytechnic Institute, Lisbon, Portugal
[2]Health & Technology Research Centre (H&TRC), Lisbon School of Health Technology, Lisbon Polytechnic Institute, Lisbon, Portugal

[Received 2 VIII 2025; Accepted 25 IX 2025]

Abstract

Introduction: Bone scintigraphy (BS) has emerged as a non-invasive technique of increasing importance in the diagnosis of transthyretin cardiac amyloidosis (CA). The most commonly used approaches include visual grading and semi-quantitative analysis. However, these techniques are limited by operator dependence and subjectivity in interpretation. To address these challenges, absolute quantification techniques are being explored to enhance diagnostic accuracy and consistency and to minimize interobserver variability. The objective is to identify the quantification methods currently employed in the assessment of CA.

Material and methods: A systematic review was conducted, including 12 articles retrieved from Scopus, PubMed, and Web of Science databases. Studies published in the last 5 years were selected, focusing on quantification methods applied to planar imaging and single photon emission computed tomography combined with computed tomography (SPECT/CT) in the context of CA.

Results: All 12 selected studies (100%) utilized visual grading; semi-quantitative methods were reported in 91.7% of studies, while absolute quantification techniques were applied in 33.3%. Among the semi-quantitative methods, the heart-to-contralateral lung (H/CL) ratio was the most commonly reported, with similar cut-off values (± 1.5) in the different articles. Additional ratios [heart-to-rib (H/R), heart-to-whole-body (H/WB), heart-to-pelvis (H/P), ratio of heart-to-thigh (RHT)] appeared less frequently, though they were investigated as alternative diagnostic markers. Absolute quantification methods reported heterogeneous cut-off thresholds, ranging from 1.25 to 6.1, based on standardized uptake values (SUVs), to discriminate between individuals with and without CA.

Conclusion: Visual grading remains the clinical standard approach. The H/CL ratio is the most reported semi-quantitative method, although it presents some limitations. Absolute quantification with SPECT/CT (SUV_{max}, SUV_{peak}) is promising for diagnosis, prognosis, and monitoring of transthyretin amyloidosis (ATTR) CA, yet consensus reference values are lacking.

KEYwords: cardiac amyloidosis (CA); transthyretin amyloidosis; bone scintigraphy; visual score; semi-quantification; absolute quantification; planar and whole-body imaging; SPECT/CT

Nucl Med Rev 2025; 28: 118–127

Introduction

Cardiac amyloidosis (CA) is a progressive, life-threatening disorder characterized by the extracellular deposition of misfolded protein fibrils, known as amyloid, within the myocardium. The two most prevalent forms are light-chain (AL) amyloidosis and transthyretin (ATTR) amyloidosis, each defined by its specific precursor protein [1–3].

In AL amyloidosis, the misfolded protein consists of monoclonal immunoglobulin light chains, typically secreted by clonal plasma cells within the bone marrow. This subtype is associated with a rapidly progressive clinical course and, in the absence of treatment, carries a median survival of less than six months [1, 2]. ATTR amyloidosis is caused by the misfolding of transthyretin (TTR), a serum transport protein for thyroxine and retinol-binding protein, primarily synthesized in the liver. It may occur due to wild-type TTR (ATTRwt)

Correspondence to: José Manuel Belo Ferreira,
Lisbon School of Health Technology, Lisbon Polytechnic Institute,
Av. D. João II, Lote 4.69.01, 1990–096 Lisbon, Portugal
tel.: +351 913 106 031, e-mail: josebeloo3@gmail.com

or hereditary variants (ATTRv) due to pathogenic TTR gene mutations. This form of CA typically presents with an age-dependent onset and progression, with clinical manifestations becoming more evident with advancing age. ATTRwt is the predominant subtype of ATTR-related CA. The various forms of amyloid deposition demonstrate marked heterogeneity in clinical course, significantly impacting both prognosis and therapeutic strategies [4].

The diagnosis of CA remains challenging, largely due to its rarity and the nonspecific nature of its clinical manifestation, which often mimics other causes of myocardial thickening, such as hypertension, chronic kidney disease, hypertrophic cardiomyopathy, and aortic stenosis. Additional barriers to timely diagnosis include limited awareness of the diagnostic algorithm and the historical lack of disease-modifying therapies [1, 5].

The diagnosis of CA typically involves cardiac magnetic resonance imaging (CMR) or echocardiography (EC), in conjunction with endomyocardial biopsy (EMB), followed by mass spectrometry or immunohistochemistry for amyloid typing [6–9]. Endomyocardial biopsy carries significant procedural risks and is typically reserved for specialized centers [6, 10]. Non-invasive modalities such as EC and CMR, although useful, lack specificity for the definitive diagnosis of CA [11, 12]. In this context, bone scintigraphy (BS) has emerged as a specific, widely accessible, and non-invasive tool for the diagnosis of ATTR-CA [6, 8, 9, 11].

BS is a highly sensitive imaging modality (sensitivity ~96%, specificity ~75%) that detects areas of increased bone and soft tissue metabolism associated with osteoblastic activity, following the administration of ^{99m}Tc-labeled diphosphonates. The exact mechanism of radiotracer uptake in the myocardium in cases of ATTR CA remains unclear. It is proposed that the radiopharmaceutical binds directly to amyloid fibrils or to adjacent microcalcifications, given its known calcium-binding properties [4, 13]. Myocardial uptake of these radiotracers is typically absent in patients without CA or prior myocardial infarction. Therefore, BS enables the differentiation of ATTR CA from other conditions that may present with similar clinical or imaging features [1, 13]. The diagnosis of ATTR CA without EMB is considered reliable only when cardiac uptake on BS is graded 2 or 3, evidence of heart failure is observed on EC or cardiac MRI, and there is no detectable monoclonal protein by serum free light chain assay and urine or serum immunofixation electrophoresis [8, 14].

Currently, two primary approaches are used in clinical practice to assess myocardial uptake of bisphosphonates: visual grading of planar and SPECT/CT images, and semi-quantitative analysis of planar scintigraphy. Both methods are endorsed by the American Society of Nuclear Cardiology and are incorporated in consensus recommendations developed by experts from multiple scientific societies specializing in multimodal imaging of CA [1, 15]. The first approach entails visual grading of myocardial uptake relative to the ribs on planar and SPECT/CT images [1, 15, 16]. This assessment is based on the Perugini scale, which categorizes radiotracer uptake into four grades: grade 0 (no myocardial uptake), grade 1 (myocardial uptake less than ribs), grade 2 (myocardial uptake equal to ribs), and grade 3 (myocardial uptake greater than ribs). Grades 2 and 3 are considered positive for CA [1, 15–17]. However, this method has several limitations, including false-positive results caused by radiotracer uptake in rib fractures or blood pool activity being mistaken for myocardial uptake related to CA [18]. Moreover, this technique does not enable assessment of disease progression or risk stratification and is susceptible to interobserver variability in visual interpretation [6, 19].

In light of these limitations, an alternative approach was developed to improve both diagnostic accuracy and risk stratification beyond that provided by visual grading [17, 19]. This method involves calculating the ratio between the mean counts in the cardiac region of interest (ROI) and the mean counts in the contralateral lung ROI [heart-to-contralateral lung (H/CL) ratio] to determine the presence or absence of CA [1, 16]. However, this technique is limited in its ability to monitor treatment response, guide therapy selection, detect early-stage CA or evaluate extracardiac tracer uptake [17, 19]. Additionally, inaccurate delineation of regions of interest (ROIs) in the H/CL ratio calculation can result in false-negative or false-positive findings [19].

Single-photon emission computed tomography combined with computed tomography (SPECT/CT) has emerged as a complementary imaging modality to BS offering enhanced specificity in the evaluation of CA [12]. This technique offers several advantages, including a reduction in false positives by distinguishing myocardial radiotracer uptake from blood pool activity, enhanced diagnostic accuracy, and improved reproducibility. By minimizing false positives, SPECT/CT increases the positive predictive value and enables precise anatomical localization of tracer uptake, as well as quantification of extracardiac uptake in soft tissues — an important factor for the prognosis of ATTR CA [12, 17, 19]. Advancements in technology and the need for more objective quantification methods in CA have led to the emergence of several absolute quantification techniques, notably the standardized uptake value (SUV), which can be utilized in SPECT/CT studies [12, 17].

Quantification methods in SPECT/CT allow correlation with disease extent and progression, facilitating early diagnosis and more accurate prognosis, while aiding treatment decisions and monitoring of ATTR CA [19]. The most widely studied metrics include maximum SUV (SUV_{max}), mean SUV (SUV_{mean}), and peak SUV (SUV_{peak}), which help differentiate ATTR CA from other cardiac conditions [20–22]. However, these methods may lead to misinterpretation in patients exhibiting low or absent radiotracer uptake, as they depend on threshold-based isocontours or manually delineated volumes of interest (VOI). Additionally, their reliance on proprietary software limits widespread implementation across institutions [7].

Despite the increasing adoption of these techniques, considerable heterogeneity exists in protocols, extracted parameters, and result interpretation, impeding inter-study comparisons and standardized clinical application. Therefore, given the inherent limitations of various quantification methods in CA it is essential to identify and compare these approaches to determine which approaches are optimized, reproducible, and clinically relevant for the diagnosis and treatment monitoring of ATTR CA.

Therefore, this systematic review aims to identify the quantification methods employed in CA. Specifically, the following objectives were established:

— to identify the quantification methods applied to planar imaging and SPECT/CT modalities;
— to identify the absolute quantification parameters utilized in SPECT/CT.

Material and methods

A systematic review was conducted on observational studies focusing on the application of quantification methods in SPECT/CT, whole-body, and/or planar BS images within the context of CA. The review followed the Preferred Reporting Items for Systematic Reviews and Meta-Analyses (PRISMA) guidelines, comprising four stages: identification, screening, eligibility, and inclusion, as outlined in Figure 1 [23]. The study protocol was submitted to PROSPERO (ID 1075977), with registration currently pending [24].

Inclusion and exclusion criteria were defined using the Population, Intervention, Comparison, Outcome (PICO) framework, as detailed in Table 1.

Articles were excluded if they did not address quantification of CA, if planar BS, whole-body scans (WBS), and/or SPECT/CT were performed using radiopharmaceuticals other than ^{99m}Tc-labelled bisphosphonates, or if they lacked visual grading of WBS, planar, and/or SPECT/CT images, semi-quantitative analysis of planar and SPECT/CT images, or absolute quantification using SPECT/CT. Additionally, articles published more than five years ago, studies without clinical performance evaluation of quantification methods, review articles, meta-analyses, and conference abstracts were excluded.

By applying strict inclusion criteria — such as limiting the analysis to studies using ^{99m}Tc-labelled bisphosphonates and excluding those without quantitative imaging — the authors aimed to ensure methodological consistency. However, these exclusions may have led to the omission of studies that, while not fully aligned with the present criteria, could still offer valuable insights into imaging practices or quantification approaches in CA. As such, the conclusions of this review are necessarily limited to a specific subset of the available literature, and caution should be exercised when generalizing these findings to broader clinical or research contexts.

The literature search was performed across three databases — Scopus, Web of Science, and PubMed — using the search strategies detailed in Table 2. Articles published from 2020 to 2025 were included, with the final search conducted on May 1, 2025. A five-year publication window was established to ensure that the included studies reflect the most current advancements and evidence

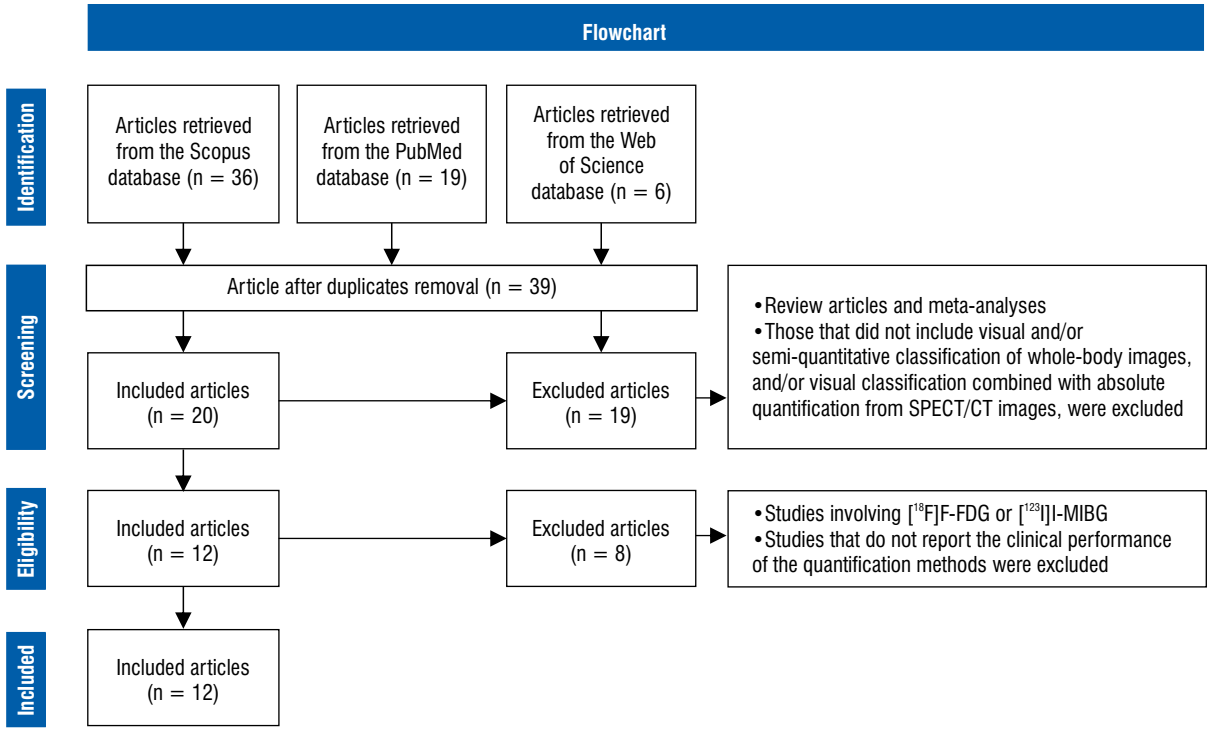

Figure 1. Distribution of quantification methods used in the articles included in the review

Table 1. PICO framework

Indicators		Inclusion criteria
P	Population	Patients with suspected or confirmed CA who underwent BS and SPECT/CT
I	Intervention	Visual classification of planar, whole-body, and/or SPECT/CT images, along with semi-quantitative analysis of planar and/or SPECT/CT images
C	Comparison	Absolute quantification of SPECT/CT images
O	Outcome	Identification and characterization of quantification methods used in BS — including planar, whole-body, and SPECT/CT imaging — in the context of CA

BS — bone scintigraphy; CA — cardiac amyloidosis; SPECT/CT — single photon emission computed tomography/computed tomography

Table 2. Databases and search equations

Databases	Search equations
Scopus	((TITLE-ABS-KEY (“spect/ct”) OR TITLE-ABS-KEY (“spect ct”) OR TITLE-ABS-KEY (“spect-ct”) OR TITLE-ABS-KEY (“quantitative spect ct”) OR TITLE-ABS-KEY (“single photon emission computed tomography”) OR TITLE-ABS-KEY (“single photon emission computed tomography computed tomography”))) AND ((TITLE-ABS-KEY (“visual score”) OR TITLE-ABS-KEY (“visual classification”) OR TITLE-ABS-KEY (semiquantitative) OR TITLE-ABS-KEY (“quantitative analysis”) OR TITLE-ABS-KEY (quantification))) AND ((TITLE-ABS-KEY (“bone scintigraphy”) OR TITLE-ABS--KEY (“bone scan”) OR TITLE-ABS-KEY (“planar imaging”))) AND ((TITLE-ABS-KEY (“cardiac amyloidosis”) OR TITLE-ABS-KEY (“transthyretin amyloidosis”) OR TITLE-ABS-KEY (“hereditary transthyretin amyloidosis”) OR TITLE-ABS-KEY (“familial transthyretin cardiac amyloidosis”))) AND PUBYEAR > 2019 AND PUBYEAR < 2026
PubMed	((((((cardiac amyloidosis[Title/Abstract]) OR (transthyretin amyloidosis[Title/Abstract])) OR (hereditary transthyretin amyloidosis[Title/Abstract])) OR (Familial Transthyretin Cardiac Amyloidosis[Title/Abstract])) AND (((bone scintigraphy[Title/Abstract]) OR (bone scan[Title/Abstract])) OR (planar imaging[Title/Abstract]))) AND (((((visual score[Title/Abstract]) OR (visual classification[Title/Abstract])) OR (semiquantitative[Title/Abstract])) OR (quantification[Title/Abstract])) OR (quantitative analysis[Title/Abstract]))) AND ((((((SPECT/CT[Title/Abstract]) OR (SPECT-CT[Title/Abstract])) OR (SPECT CT[Title/Abstract])) OR (quantitative SPECT CT[Title/Abstract])) OR (single photon emission computed tomography [Title/Abstract])) OR (Single Photon Emission Computed Tomography Computed Tomography[MeSH Terms])) Filters: from 2020–2025
Web of Science	(((((TS = (“spect/ct”)) OR TS = (“spect ct”)) OR TS = (“spect-ct”)) OR TS = (“quantitative spect ct”)) OR TS = (“single photon emission computed tomography”)) OR TS = (“single photon emission computed tomography computed tomography”) AND ((((TS = (“visual score”)) OR TS = (“visual classification”)) OR TS = (semiquantitative)) OR TS = (quantification)) OR TS = (“quantitative analysis”) AND ((TS = (“bone scan”)) OR TS = (“planar imaging”)) OR TS = (“bone scintigraphy”) AND ((TS = (“transthyretin amyloidosis”)) OR TS = (“cardiac amyloidosis”)) OR TS = (“hereditary transthyretin amyloidosis”)

Table 3. Classification of article quality and journal quartiles

Authors	Journals	Methodological quality (JBI, 0–10)	SJR (Q)
Kessler et al. (2022) [7]	J Nucl Cardiol	7.7	Q2
Scully et al. (2020) [25]	JACC Cardiovasc Imaging	7.7	Q1
Singh et al. (2020) [26]	J Nucl Cardiol	8.7	Q2
Mallón Araujo et al. (2023) [27]	Imagen Mol (Engl Ed)	8.7	Q3
Avalon et al. (2022) [28]	J Nucl Cardiol	8	Q2
Ionescu et al. (2024) [29]	Med Surg J	7.7	Q1
Campi et al.(2023) [30]	J Cardiovasc Dev Dis	7.7	Q1
Coskun et al. (2022) [31]	Int J Cardiovasc Imaging	8.3	Q2
Minutoli et al. (2022) [32]	Eur Radiol	8.3	Q1
Asif et al.(2020) [33]	J Nucl Cardiol	7	Q2
Small et al. (2021) [34]	J Nucl Cardiol	8	Q2
Caobelli et al. (2020) [35]	J Nucl Cardiol	8	Q2

JBI — Joanna Briggs Institute Critical Appraisal Tools; SJR — SCImago Journal Rank; Q — quartile

in the rapidly evolving field of SPECT/CT technology in medical imaging, thereby enhancing the review's capacity to address its objectives with up-to-date and clinically relevant data.

As illustrated in Figure 1, a total of 58 articles were retrieved, of which 19 duplicates were removed. The remaining 39 articles were screened according to the predefined criteria, resulting in the exclusion of 19 studies. Consequently, 12 articles were included in the final analysis. Study selection was performed independently by two reviewers based on predefined eligibility criteria. Studies were initially excluded based on their title and abstract, and the remaining articles underwent full-text analysis. Discrepancies were resolved through discussion until consensus was reached, resulting in the final selection of studies included in the systematic review.

As shown in Table 3 [7, 25–35], the quality of the selected articles was assessed using the Joanna Briggs Institute Critical Appraisal Tools (JBI) Checklist for Diagnostic Test Accuracy Studies [36]. Two authors (JB and MN) independently reviewed all articles, rating each item as “Yes”, “No”, or “Uncertain”; All assessments were independently conducted, and discrepancies were resolved through discussion until consensus was reached. Final scores for each article were calculated by summing the assigned values (“No” = 1, “Uncertain” = 2, “Yes” = 3) and converting the total to a nominal scale from 0 to 10. Additionally, the quartile

ranking of the journal in which each article was published was determined according to the SCImago Journal Rank (SJR), based on the relevant scientific field [37].

Results

The articles selected for this review aim to identify and compare the most optimized, reproducible quantification methods for diagnosing CA using BS and SPECT/CT examinations. Table 4 [7, 25–35] summarizes the 12 eligible studies, detailing author, publication year, study design, sample size, objectives, and key findings.

As shown in Table 5, the imaging techniques used in the studies and their corresponding quantification methods were identified. Figure 2 illustrates the proportions of qualitative and quantitative classification methods employed in the selected articles. Figure 3 presents the cut-off values for the H/CL ratio and SUV in the diagnosis of CA, respectively.

Table 6 [7, 25, 28, 35] summarizes the absolute SUV values (mean ± SD) in CA and N/CA groups, along with the cut-off thresholds used to distinguish between them. Across studies, SUV values were consistently higher in CA patients. Notably, Scully et al. [25] employed SUV_{peak} as the metric, whereas others used SUV_{max}.

Discussion

This systematic review identified the main quantification methods used to evaluate patients with suspected or confirmed CA using BS. Visual grading was employed in all studies (100%), followed by semi-quantitative analysis in 91.7% of studies, while absolute quantification using SPECT/CT was less common, reported in 33.3% of the studies, as shown in Figure 2.

Visual grading remains the most widely employed method for diagnosing CA (Fig. 2). Nonetheless, emerging image quantification techniques are increasingly incorporated into clinical research and practice (Tab. 4), aiming to overcome the known limitations of visual assessment — such as false positives, interobserver variability, and the inability to perform risk stratification. Despite concerns regarding inter- and intra-observer variability, Singh et al. [26] reported complete agreement (100%) in the visual grading of patient images, both between different observers and within the same observer. However, this agreement was based on the binary classification of planar images as either positive or negative, without distinguishing the extent of CA as defined by the Perugini grading scale [26].

To reduce operator dependence associated with visual classification, semi-quantitative methods — particularly the heart-to-contralateral lung (H/CL) ratio — have been implemented, enhancing objectivity and reproducibility in image analysis. This method demonstrates high sensitivity and moderate specificity (Tab. 4). The study by Asif et al. [33] demonstrated that combining visual classification with the H/CL ratio reduced sensitivity from 98% to 57%, highlighting diagnostic errors associated with this semi-quantitative method. The authors found that the H/CL ratio misclassified the degree of CA in more cases than visual assessment alone. This discrepancy may be attributed to false positives resulting from pleural and/or pericardial effusions, as well as calcifications in the aortic and/or mitral valves, which can increase counts within the defined ROIs for the heart and contralateral lung, thereby elevating the H/CL ratio. Conversely, myocardial infarction may lead to a decreased H/CL ratio due to reduced tracer uptake in the heart ROI.

In Scully et al. [25], differentiating between grades 2 and 3 on the Perugini scale using the H/CL ratio is challenging, as soft-tissue uptake adjacent to the heart interferes with count accuracy within the defined ROIs. The studies by Glavam et al. [38] and Aziz et al. [39] also refer that anatomical variations and extracardiac radiopharmaceutical uptake may further compromise the reliability of this method, potentially leading to false-positive and false-negative results. However, unlike visual classification, the H/CL ratio enables prognostic assessment in individuals with ATTR CA offering clinical value in predicting disease progression, which visual methods alone cannot reliably provide [40]. The clinical application of this semi-quantitative method relies on standardized and well-defined cut-off values for the diagnosis of CA which are dependent on the timing of image acquisition following radiopharmaceutical administration [1]. Figure 3 presents the cut-off values for the H/CL ratio in planar images acquired at 1 hour, highlighting a prevailing threshold of ≥ 1.5, above which CA is considered positive. However, it is not recommended to rely on H/CL ratio values for diagnosing CA in the absence of myocardial radiopharmaceutical uptake on SPECT imaging [1]. In the absence of SPECT imaging, the study by Ionescus et al. [29] found that the heart-to-rib ratio (H/R), combined with visual classification and the H/CL ratio, facilitates accurate diagnosis of CA.

To address the limitations of the H/CL ratio, alternative semi-quantitative approaches have been investigated (Tab. 5). For example, Campi et al. [30] employed three semi-quantification metrics: heart-to-thigh ratio (RHT), contralateral lung-to-thigh ratio (RLT), and femur-to-thigh ratio (RFT). The thigh was selected as a reference region due to its minimal radiopharmaceutical uptake in CA, reducing confounding from extracardiac activity that may affect H/CL ratio quantification. The heart-to-thigh (RHT) ratio showed superior performance [area under the curve (AUC) = 0.96] in distinguishing patients with CA from controls, serving as a valuable adjunct to visual classification in ambiguous cases. However, its clinical utility may be limited by potential confounding factors such as patient age and sex [30].

The study by Small et al. [34] proposed two alternative semi-quantitative methods for diagnosing CA: the heart-to-whole-body ratio (H/WB) and the heart-to-pelvis ratio (H/P). The H/WB ratio demonstrated excellent diagnostic performance, with both sensitivity and specificity at 100%, enhancing the detection of CA and enabling differentiation between patients with grade 1 and grade 2 ATTR CA according to the Perugini scale [34].

Recent studies by Al Taha et al. [41] and Watanabe et al. [42] have demonstrated that SPECT/CT imaging significantly enhances the diagnostic accuracy of CA. This imaging modality reduces ambiguous CA findings, improves reproducibility, allows for absolute quantification metrics, provides attenuation correction, and enhances anatomical localization accuracy [7, 12, 17, 19, 31]. The study by Coskun et al. [31] reported a weak to moderate agreement between the semi-quantitative H/CL ratio on planar imaging and visual SPECT/CT classification, highlighting the limitations of planar imaging when relying on the H/CL ratio in accurately grading CA compared to SPECT/CT.

The images obtained through SPECT/CT facilitated the application of absolute quantification methods, including SUV_{max}, SUV_{peak},

Table 4. Characteristics of the selected studies

Authors	Study type	Study sample	Objective	Results
Kessler et al. (2022) [7]	Observational, analytical, cross-sectional, retrospective, and non-randomized	Individuals with ATTR CA (n = 136)	To implement a quantification method using SPECT/CT images and compare it with visual classification	AUC for CA: 0.81 ± 0.04 (p = 0.0001) AUC for ATTR subtype: 0.96 ± 0.02 (p = 0.0001) SUV_{max} (sensitivity and specificity): 98.7% and 87.2%, respectively (p < 0.0001)
Scully et al. (2020) [25]	Observational, analytical, cross-sectional, retrospective, and non-randomized	Individuals with ATTR CA (n = 100)	Evaluate whether quantification through SPECT/CT images improves diagnostic accuracy	SUV_{peak} and SUV retention index (sensitivity and specificity): 100% and 75% H/CL (sensitivity and specificity): 100% and 38% AUC for SUV_{peak} and SUV retention index: 0.999 AUC for H/CL ratio: 0.987
Singh et al. (2020) [26]	Observational, cohort, and retrospective	Individuals with ATTR CA (n = 100)	Determine the inter- and intra-observer variability in the interpretation of BS for the diagnosis of ATTR CA	Intra- and inter-observer agreement was high, with correlation coefficients of r = 0.90 and 0.99 for Observer 1, and r = 0.98 between observers
Mallón Araujo et al. (2023) [27]	Observational, analytical, cross-sectional, retrospective, and non-randomized	Individuals with ATTR CA (n = 46)	Validate the use of SPECT/CT and assess whether uptake quantification allows for determining the amyloid burden	H/CL for planar imaging (sensitivity and specificity): 95.2% and 94.4% and an AUC of 0.971 H/CL for SPECT (sensitivity and specificity): 95% and 88,9% and an AUC of 0.966 (p < 0.05) Visual score (sensitivity and specificity): 95.2% and 94.7%
Avalon et al. (2022) [28]	Observational, analytical, cross-sectional, retrospective	Individuals with ATTR CA (n = 78)	Evaluate whether quantification through SPECT/CT imaging improves diagnostic accuracy	SUV_{max} 1 h (sensitivity and specificity): 67% and 98% 1.88 SUV_{max} 3 h (sensitivity and specificity): 100% and 96.7%, SUV > 1.25
Ionescus et al. (2024) [29]	Observational, analytical, cross-sectional, retrospective, and non-randomized	Individuals with ATTR CA (n = 80)	Determine the minimum number of nuclear medicine images required for an accurate diagnosis	Not applicable
Campi et al. (2023) [30]	Observational, analytical, cross-sectional, retrospective, and non-randomized	Individuals with ATTR CA (n = 68)	Evaluation of the additional information provided by a semi-quantification method of [^{99m}Tc]Tc-HMDP or [^{99m}Tc]Tc-DPD uptake compared to visual classification	RHT (sensitivity/specificity/AUC in women): 94%, 87%, and 0.96 RLT (sensitivity/specificity/AUC in women): 88%, 66%, and 0.81 RFT (sensitivity/specificity/AUC in women): 50%, 70%, and 0.59 RHT (sensitivity/specificity/AUC in men): 81%, 88%, and 0.87 RHT (sensitivity/specificity/AUC in men): 33%, 95%, and 0.67 RFT (sensitivity/specificity/AUC in men): 38%, 86%, and 0.63
Coskun et al. (2022) [31]	Observational, analytical, cross-sectional, retrospective, and non-randomized	Individuals with ATTR CA (n = 141)	Evaluate the agreement between semi-quantitative assessment in planar images and visual classification through SPECT/CT images	Agreement between SPECT/CT images and planar images at 3 hours was moderate, with a correlation coefficient of V = 0.341 and p < 0.001 Agreement between SPECT/CT images and planar images at 1 hour was moderate, with a correlation coefficient of V = 0.413 and p < 0.001
Minutoli et al. (2022) [32]	Observational, analytical, cross-sectional, retrospective, and non-randomized	Individuals with ATTR CA (n = 53)	Evaluate the clinical performance of BS with [^{99m}Tc]Tc--DPD in the early phase compared to the late phase	H/CL (sensitivity and specificity): 85.71% and 92%
Asif et al. (2020) [33]	Observational, analytical, cross-sectional, retrospective, and non-randomized	Individuals with ATTR CA (n = 133)	Comparison of findings on planar images with those on SPECT images	Sensitivity, specificity, VPP, and VPN of CV: 97%, 98%, 94%, 99%, and 98% Sensitivity, specificity, VPP, and VPN of CV with an H/CL ratio: 57%, 95%, 80%, 85%, and 85%
Small et al. (2021) [34]	Observational, analytical, and non-randomized	Individuals with ATTR CA (n = 76)	Application of six different quantitative methods to measure myocardial uptake of [^{99m}Tc]Tc-HMDP	H/P (sensitivity and specificity): 95% and 100% H/CL(sensitivity and specificity): 98% and 100% H/WB (sensitivity and specificity): 100% and 100%
Caobelli et al. (2020) [35]	Observational, analytical, cross-sectional, retrospective, and non-randomized	Individuals with ATTR CA (n = 13)	Assessment of the validity of quantitative evaluation and correlation of the different parameters with visual classification	Not applicable

ATTR — transthyretin amyloidosis; AUC — area under the curve; BS — bone scintigraphy; CA — cardiac amyloidosis; CV — coefficient of Variation; H/CL — heart-to-contralateral lung ratio; H/P — heart-to-pelvis ratio; H/WB — heart-to-rib ratio; RHT — ratio of heart-to-thigh; RLT — lung to thigh ratio; RFT — femur-to-thigh ratio; SPECT/CT — single photon emission computed tomography/computed tomography; SUV_{max} — maximum standardized uptake value; SUV_{peak} — peak standardized uptake value; VPN — valor predictive negative; VPP — valor predictive positive

Table 5. Imaging techniques and corresponding quantification methods

Image acquisition techniques	Quantification methods
Planar imaging	Visual classification using the Perugini scale and/or semi-quantitative assessment (H/CL, H/WB, H/P, H/R, RHT, RLT, RFT)
Whole body	Visual classification using the Perugini scale and/or semi-quantitative assessment (H/WB)
SPECT/CT	SUV_{max}, SUV_{peak}, Myocardial Retention Index, and/or H/CL ratio

H/CL — heart-to-contralateral lung ratio; H/WB — heart-to-whole body ratio; H/P — heart-to-pelvis ratio; H/R — heart-to-rib ratio; RHT — heart-to-thigh ratio; RLT — contralateral lung ratio

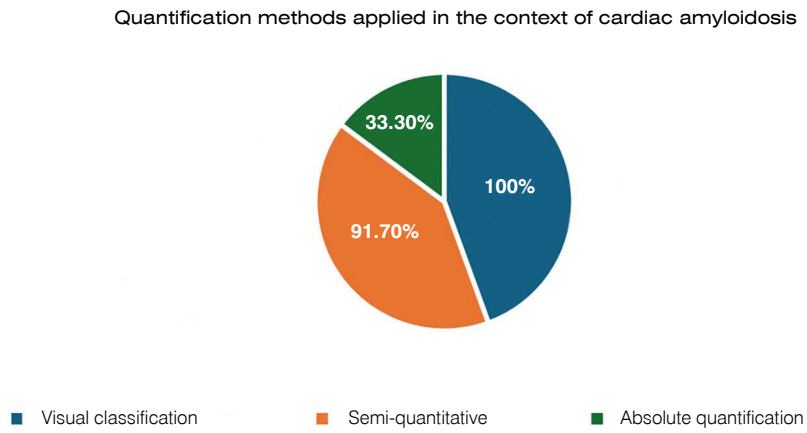

Figure 2. Distribution of quantification methods used in the articles included in the review

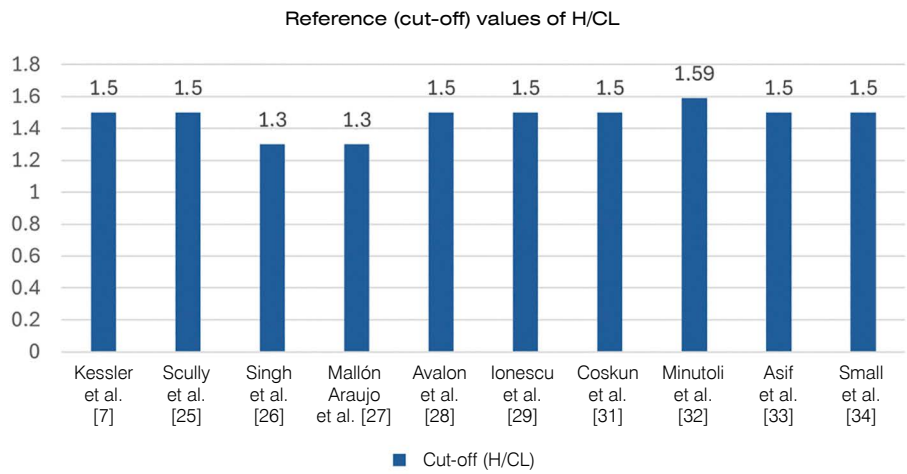

Figure 3. Graph representing the cut-off point for the H/CL of planar images at 1 hour in the diagnosis of cardiac amyloidosis; H/CL — heart-to--contralateral lung ratio

Table 6. Absolute SUV values for CA and N/CA and respective SUV cut-off values

Authors	SUV metric	N/CA	CA	Cut-off values
Kessler et al. (2023) [7]	SUV_{max}	3.25 ± 1.01	15.0 ± 2.7	6.1
Scully et al. (2020) [25]	SUV_{peak}	1.00 ± 0.40	8.73 ± 1.45	1.7
Avalon et al. (2023) [28]	SUV_{max}	0.00	1.14 ± 0.58	1.25
Caobelli et al. (2020) [35]	SUV_{max}	2.42	16.15	3.3

CA — cardiac amyloidosis, N/CA — non-cardiac amyloidosis; SUV — standardized uptake value

and mean standardized uptake value (SUV_{mean}) [17]. According to studies by Kessler et al. [7], Scully et al. [25], and Avalon et al. [28], these metrics demonstrated high sensitivity (98.7–100%) and moderate to high specificity (75–96.7%) [42]. Specifically, Kessler et al. [7] and Scully et al. [25] concluded that SUV_{max} and SUV_{peak}, respectively, enable accurate differentiation between individuals with and without CA, with AUC values of 0.96 and 0.99, respectively. Furthermore, according to Kessler et al. [7], absolute quantification methods allow estimation of amyloid burden, enhancing diagnosis, evaluation of treatment response, and risk stratification.

However, these absolute quantification methods remain infrequently used in clinical practice, primarily due to the absence of standardized reference values and the need for further validation in the diagnosis of CA [27]. Different studies use varying threshold values for the SUV cut-off above which CA is considered positive, as illustrated in Table 6. These thresholds correspond to the absolute SUV values, which reveal significant variability between patients without CA (N/CA) and those with CA. This variation in SUV values can be attributed to multiple factors affecting the metric, including the concentration of the radiopharmaceutical in the tissue and the administered activity, both of which differ across studies. Supporting this, Halim et al. [43] suggest that lower activity concentrations yield more accurate SUV measurements compared to higher concentrations. In addition to these factors, SUV measurements can be influenced by the specific equipment used, the filtering techniques applied, and the reconstruction protocols of the acquired images. Kabos et al. [44] emphasize that different SPECT/CT systems utilize varying reconstruction algorithms and parameters. Consequently, the number of iterations and subsets differs between devices, where increasing the number of iterations enhances spatial resolution but also raises image noise, ultimately impacting the SUV_{max} values [21, 44]. Regarding the filters applied during image post-processing, studies by Lyra et al. [45] and Myint et al. [46] report that increasing the cut-off frequency of low-pass filters results in higher spatial resolution and image noise, which in turn elevates both SUV_{max} and SUV_{mean} values.

As noted by Scully et al. [25] and Caobelli et al. [35], distinguishing Perugini grades 2 and 3 using SUV_{peak} and SUV_{max} is limited by radiopharmaceutical uptake in adjacent soft tissues. To overcome this, alternative quantitative metrics — SUV retention index, normalized maximum standardized uptake value ($nSUV_{max}$), and normalized peak standardized uptake value ($nSUV_{peak}$) — have been introduced. According to Rettl et al. [47], the SUV retention index enhances diagnostic accuracy by accounting for radiopharmaceutical uptake in the paravertebral and vertebral muscles, thereby minimizing interference from extracardiac uptake. Wollenweber et al. [48] reported overlapping SUV_{peak} values between Perugini grades 2 and 3, with higher values observed in some grade 2 cases. This counterintuitive finding was attributed to competitive radiopharmaceutical uptake among bone, myocardium, and adjacent soft tissues in grade 3 patients. The authors proposed normalizing SUV values using a bone-based volume of interest (VOI) to mitigate anatomical artifacts and enhance diagnostic accuracy [48].

Currently, novel quantification methods such as cardiac amyloid activity (CAA) and percentage of injected dose (%ID) are being investigated. These metrics facilitate the assessment of treatment response and risk stratification by providing a more comprehensive representation of amyloid burden. Unlike SUV_{max} and SUV_{peak}, CAA and percentage of injected dose (%ID) take into account both myocardial volume and radiopharmaceutical uptake intensity, offering a potentially more accurate reflection of disease extent [20, 49].

This systematic review has some limitations, primarily the limited number of studies employing absolute quantification methods. As a relatively recent approach, its clinical application and scientific validation are still in the early stages of consolidation. Additionally, the time range selected for the literature search may have been too narrow. A broader search period — exceeding five years — could have allowed the inclusion of other studies, potentially providing a more comprehensive overview of the evolution and application of absolute quantification in nuclear medicine. The widespread use of visual and semi-quantitative methods, driven by their simplicity and standardized criteria, has limited the exploration of more precise quantitative techniques. Additionally, the absence of diagnostic performance metrics in some studies hinders the comparative assessment of accuracy and reproducibility among the available methods for diagnosing CA. Furthermore, this review was limited by its exclusion of studies that did not meet strict methodological criteria, including older publications, non-original articles, or studies not using ^{99m}Tc-labelled bisphosphonates. Furthermore, studies without quantification methods or clinical performance assessment were excluded. These exclusions, although necessary for methodological rigor, may limit the generalizability of the findings and exclude relevant insights from a broader body of literature.

Conclusions

This systematic review identified the main quantification methods used to assess CA through BS, demonstrating that visual grading remains the most commonly applied approach in clinical practice despite its limitations. Semi-quantitative methods, particularly the heart-to-contralateral lung (H/CL) ratio, offer a more objective alternative for diagnosis, although their accuracy can be affected by anatomical factors. Additionally, other semi-quantitative metrics show promise for CA assessment but require further clinical validation.

In SPECT/CT, absolute quantification metrics such as SUV_{max} and SUV_{peak} have been recognized as important tools for prognosis, diagnosis, therapy monitoring, and risk stratification in ATTR CA. However, the lack of standardized protocols and reference values currently restricts their widespread clinical application, highlighting the need for further validation and standardization studies.

Article information and declarations

Acknowledgments

The authors of this paper express their sincere gratitude to Professor Sérgio Figueiredo for his guidance, availability, and dedication throughout the entire process.

Author contributions

All authors contributed to this systematic review.

Funding

No external funding.

Conflicts of interest

The authors declare no conflict of interest.

Supplementary material

The Supplementary Material for this article can be found online at https://journals.viamedica.pl/nuclear_medicine_review/article/view/107884.

References

1. Dorbala S, Ando Y, Bokhari S, et al. ASNC/AHA/ASE/EANM/HFSA/ISA/SCMR/SNMMI expert consensus recommendations for multimodality imaging in cardiac amyloidosis: part 1 of 2-evidence base and standardized methods of imaging. J Nucl Cardiol. 2021; 14(7): e000029, doi: 10.1161/HCI.0000000000000029, indexed in Pubmed: 34196223.
2. Dorbala S, Bokhari S, Glaudemans A, et al. ASNC AND EANM cardiac amyloidosis practice points: 99mTechnetium-3,3-diphosphono-1,2-propanodicarboxylic acid (DPD) and 99mTechnetium-hydroxymethylene diphosphonate (HMDP) imaging for transthyretin cardiac amyloidosis. American Society of Nuclear Cardiology & European Association of Nuclear Medicine. 2019; 1st ed. https://www.asnc.org/wp-content/uploads/2024/05/19110-ASNC-AND-EANM-Amyloidosis-Practice-Points-WEB2-2.pdf (2.08.2025).
3. Bloom MW, Gorevic PD. Cardiac amyloidosis. Ann Intern Med. 2023; 176(3): ITC33–ITC48, doi: 10.7326/AITC202303210, indexed in Pubmed: 36913688.
4. Lewkowicz E, Jayaraman S, Gursky O. Molecular basis for non-invasive diagnostics of cardiac amyloids using bone tracers. Biomater Sci. 2024; 12(17): 4275–4282, doi: 10.1039/d4bm00816b, indexed in Pubmed: 39046441.
5. Huang He, Liu Y, Chen X, et al. Analysis and insights of cardiac amyloidosis: novel perception of rare diseases in cardiology. Am J Transl Res. 2024; 16(9): 4534–4548, doi: 10.62347/KXHZ6884, indexed in Pubmed: 39398585.
6. Castaño A, DeLuca A, Weinberg R, et al. Serial scanning with technetium pyrophosphate (Tc-PYP) in advanced ATTR cardiac amyloidosis. J Nucl Cardiol. 2016; 23(6): 1355–1363, doi: 10.1007/s12350-015-0261-x, indexed in Pubmed: 26453570.
7. Kessler L, Fragoso Costa P, Kersting D, et al. Quantitative Tc-DPD-SPECT/CT assessment of cardiac amyloidosis. J Nucl Cardiol. 2023; 30(1): 101–111, doi: 10.1007/s12350-022-02960-3, indexed in Pubmed: 35562639.
8. Ren C, Ren J, Tian Z, et al. Assessment of cardiac amyloidosis with Tc-pyrophosphate (PYP) quantitative SPECT. EJNMMI Phys. 2021; 8(1): 3, doi: 10.1186/s40658-020-00342-7, indexed in Pubmed: 33411102.
9. Ogasawara K, Shiraishi S, Tsuda N, et al. Usefulness of quantitative Tc--pyrophosphate SPECT/CT for predicting the prognosis of patients with wild-type transthyretin cardiac amyloidosis. Jpn J Radiol. 2022; 40(5): 508–517, doi: 10.1007/s11604-021-01221-6, indexed in Pubmed: 34973114.
10. Li ZP, Li GL, Wang YN, et al. Endomyocardial biopsy: short- and long-term safety in myocarditis patients. Cardiology. 2025: 1–14, doi: 10.1159/000543593, indexed in Pubmed: 39842418.
11. Dorbala S, Kijewski MF, Park MA. Quantitative bone-avid tracer SPECT/CT for cardiac amyloidosis: a crucial step forward. JACC Cardiovasc Imaging. 2020; 13(6): 1364–1367, doi: 10.1016/j.jcmg.2020.05.005, indexed in Pubmed: 32498922.
12. Paeng JC, Choi JY. Nuclear imaging for cardiac amyloidosis: bone scan, SPECT/CT, and amyloid-targeting PET. Nucl Med Mol Imaging. 2021; 55(2): 61–70, doi: 10.1007/s13139-020-00681-4, indexed in Pubmed: 33968272.
13. Nebhwani M, Chaibekava K, Achten A, et al. Detection of cardiac amyloidosis on routine bone scintigraphy: an important gatekeeper role for the nuclear medicine physician. Int J Cardiovasc Imaging. 2024; 40(6): 1183–1192, doi: 10.1007/s10554-024-03085-z, indexed in Pubmed: 38520623.
14. Gillmore JD, Maurer MS, Falk RH, et al. Nonbiopsy diagnosis of cardiac transthyretin amyloidosis. Circulation. 2016; 133(24): 2404–2412, doi: 10.1161/CIRCULATIONAHA.116.021612, indexed in Pubmed: 27143678.
15. Régis C, Harel F, Martineau P, et al. Tc-99m-pyrophosphate scintigraphy for the diagnosis of ATTR cardiac amyloidosis: Comparison of quantitative and semi-quantitative approaches. J Nucl Cardiol. 2020; 27(5): 1808–1815, doi: 10.1007/s12350-020-02205-1, indexed in Pubmed: 32476105.
16. Schockling EJ, Farrell MB, Embry-Dierson M, et al. Cardiac amyloidosis imaging, part 2: quantification and technical considerations. J Nucl Med Technol. 2023; 51(2): 90–98, doi: 10.2967/jnmt.123.265416, indexed in Pubmed: 37268318.
17. Auer B, Kijewski MF, Dorbala S. Quantitative ATTR-cardiac amyloidosis SPECT/CT imaging: the time is now! J Nucl Cardiol. 2023; 30(3): 1246–1249, doi: 10.1007/s12350-023-03278-4, indexed in Pubmed: 37138175.
18. Zhu Y, Pan R, Peng D, et al. Pitfalls of the semi-quantitative analyzing ^{99m}Tc-pyrophosphate planar images for diagnosing transthyretin cardiac amyloidosis: a possible solution. Diagnostics (Basel). 2022; 12(1): 94, doi: 10.3390/diagnostics12010094, indexed in Pubmed: 35054261.
19. Ayers MP, Peruri AV, Bourque JM. Transforming ATTR cardiac amyloidosis into a chronic disease: the enormous potential of quantitative SPECT to improve diagnosis, prognosis, and monitoring of disease progression. J Nucl Cardiol. 2021; 28(5): 1846–1850, doi: 10.1007/s12350-021-02587-w, indexed in Pubmed: 33851351.
20. Dorbala S, Park MA, Cuddy S, et al. Absolute quantitation of cardiac 99mTc-pyrophosphate using cadmium-zinc-telluride-based SPECT/CT. J Nucl Med. 2021; 62(5): 716–722, doi: 10.2967/jnumed.120.247312, indexed in Pubmed: 32887756.
21. Sperry BW, Bateman TM, Akin EA, et al. Hot spot imaging in cardiovascular diseases: an information statement from SNMMI, ASNC, and EANM. J Nucl Med. 2022 [Epub ahead of print], doi: 10.2967/jnumed.122.264311, indexed in Pubmed: 35863895.
22. Matsuda N, Otsuka H, Otani T, et al. New quantitative indices of cardiac amyloidosis with 99mTc-pyrophosphate scintigraphy. Jpn J Radiol. 2023; 41(4): 428–436, doi: 10.1007/s11604-022-01364-0, indexed in Pubmed: 36449252.
23. Page MJ, McKenzie JE, Bossuyt PM, et al. The PRISMA 2020 statement: an updated guideline for reporting systematic reviews. BMJ. 2021; 372(n71), doi: 10.1136/bmj.n71.
24. Centre for Reviews and Dissemination. PROSPERO: International prospective register of systematic reviews; York: University of York; 2025. https://www.crd.york.ac.uk/PROSPERO/ (17.06.2025).
25. Scully PR, Morris E, Patel KP, et al. DPD quantification in cardiac amyloidosis: a novel imaging biomarker. JACC Cardiovasc Imaging. 2020; 13(6): 1353––1363, doi: 10.1016/j.jcmg.2020.03.020, indexed in Pubmed: 32498921.
26. Singh V, Cuddy S, Kijewski MF, et al. Inter-observer reproducibility and intra-observer repeatability in 99mTc-pyrophosphate scan interpretation for diagnosis of transthyretin cardiac amyloidosis. J Nucl Cardiol. 2022; 29(2): 440–446, doi: 10.1007/s12350-020-02353-4, indexed in Pubmed: 32918247.
27. Mallón Araujo MD, Abou Jokh Casas E, Abou Jokh Casas C, et al. Description of a different quantification method for amyloid burden (DPDload) and validation of SPECT/CT in cardiac amyloidosis. Rev Esp Med Nucl Imagen Mol (Engl Ed). 2023; 42(3): 171–177, doi: 10.1016/j.remnie.2023.02.005, indexed in Pubmed: 36796676.
28. Avalon JC, Fuqua J, Deskins S, et al. Quantitative single photon emission computed tomography derived standardized uptake values on ^{99m}Tc-PYP scan in patients with suspected ATTR cardiac amyloidosis. J Nucl Cardiol. 2023; 30(1): 127–139, doi: 10.1007/s12350-022-02988-5, indexed in Pubmed: 35655113.
29. Ionescu I, Grierosu I, Ciocoiu M. Static and whole-body images vs. SPECT: together or separate for an accurate detection of transthyretin cardiac amyloidosis. Med Surg J. 2024; 128(3): 569–576, doi: 10.22551/msj.2024.03.15.
30. Campi C, Briani C, Salvalaggio A, et al. Semi-Quantification of myocardial uptake of bone-seeking agents in suspected cardiac amyloidosis. J Cardiovasc Dev Dis. 2023; 10(5), doi: 10.3390/jcdd10050184, indexed in Pubmed: 37233151.
31. Coskun N, Kartal MO, Erdogan AS, et al. Tc-99m pyrophosphate scintigraphy for cardiac amyloidosis: concordance between planar and SPECT/CT imag-

ing. Int J Cardiovasc Imaging. 2022; 38(9): 2081–2088, doi: 10.1007/s10554-022-02676-y, indexed in Pubmed: 37726620.

32. Minutoli F, Russo M, Di Bella G, et al. Diagnosis of cardiac amyloid transthyretin (ATTR) amyloidosis by early (soft tissue) phase [^{99m}Tc]Tc-DPD whole body scan: comparison with late (bone) phase imaging. Eur Radiol. 2022; 32(5): 3035–3044, doi: 10.1007/s00330-021-08420-9, indexed in Pubmed: 35031838.
33. Asif T, Gomez J, Singh V, et al. Comparison of planar with tomographic pyrophosphate scintigraphy for transthyretin cardiac amyloidosis: Perils and pitfalls. J Nucl Cardiol. 2021; 28(1): 104–111, doi: 10.1007/s12350-020-02328-5, indexed in Pubmed: 32901418.
34. Small GR, Ruddy TD. Straightening out the wrinkles in technetium-99m-labeled bone scintigraphy tracer assessment of cardiac amyloidosis. J Nucl Cardiol. 2021; 28(1): 100–103, doi: 10.1007/s12350-019-01718-8, indexed in Pubmed: 30977095.
35. Caobelli F, Braun M, Haaf P, et al. Quantitative Tc-DPD SPECT/CT in patients with suspected ATTR cardiac amyloidosis: feasibility and correlation with visual scores. J Nucl Cardiol. 2020; 27(5): 1456–1463, doi: 10.1007/s12350-019-01893-8, indexed in Pubmed: 31538322.
36. SCImago. Scimago journal & country rank [Internet].Granada: SCImago Research Group; 2007. https://www.scimagojr.com/ (25.04.2025).
37. Joanna Briggs Institute. Critical appraisal tools: tools to assess the trustworthiness, relevance and results of published papers. https://jbi.global/critical-appraisal-tools (25.04.2025).
38. Glavam A, Lopes R, Brandão S. My approach to imaging cardiac amyloidosis: role of bone-seeking tracers scintigraphy. Arq Bras Cardiol Imagem Cardiovasc. 2023; 36(2): e20230012, doi: 10.36660/abcimg.20230012i.
39. Kavita A, Onny MAA, Suppiah S, et al. A challenging road to diagnosing transthyretin cardiac amyloidosis and using technetium-99m pyrophosphate bone scintigraphy in nuclear cardiology — a case report. Med J Malaysia. 2021; 76(5): 762–767, indexed in Pubmed: 34508392.
40. Castano A, Haq M, Narotsky D, et al. Multicenter study of planar technetium 99m pyrophosphate cardiac imaging. JAMA Cardiology. 2016; 1(8): 880–889, doi: 10.1001/jamacardio.2016.2839, indexed in Pubmed: 27557400.
41. Al Taha Z, Alibazoglu D, Sabbour H, et al. Attacking the Achilles heel of cardiac amyloid nuclear scintigraphy: How to reduce equivocal and false positive studies. J Nucl Cardiol. 2023; 30(5): 1922–1934, doi: 10.1007/s12350-023-03214-6, indexed in Pubmed: 36859593.
42. Watanabe S, Nakajima K, Wakabayashi H, et al. Volumetric evaluation of Tc-pyrophosphate SPECT/CT for transthyretin cardiac amyloidosis: methodology and correlation with cardiac functional parameters. J Nucl Cardiol. 2022; 29(6): 3102–3110, doi: 10.1007/s12350-021-02857-7, indexed in Pubmed: 34907500.
43. Halim F, Yahya H, Jaafar KN, et al. Accuracy assessment of SUV measurements in SPECT/CT: a phantom study. J Nucl Med Technol. 2021; 49(3): 250–255, doi: 10.2967/jnmt.120.259168, indexed in Pubmed: 33722927.
44. Knoll P, Kotalova D, Köchle G, et al. Comparison of advanced iterative reconstruction methods for SPECT/CT. Z Med Phys. 2012; 22(1): 58–69, doi: 10.1016/j.zemedi.2011.04.007, indexed in Pubmed: 21723716.
45. Lyra M, Ploussi A. Filtering in SPECT image reconstruction. Int J Biomed Imaging. 2011; 2011: 693795, doi: 10.1155/2011/693795, indexed in Pubmed: 21760768.
46. Myint TT, Ekjeen T, Chaichana A, et al. Factors affecting standardized uptake value of ^{99m}Tc-MDP bone SPECT/CT: a phantom study. J Phys Conf Ser. 2019; 1248(1): 012026, doi: 10.1088/1742-6596/1248/1/012026.
47. Rettl R, Calabretta R, Duca F, et al. DPD quantification correlates with extracellular volume and disease severity in wild-type transthyretin cardiac amyloidosis. JACC Adv. 2024; 3(10): 101261, doi: 10.1016/j.jacadv.2024.101261, indexed in Pubmed: 39309666.
48. Wollenweber T, Rettl R, Kretschmer-Chott E, et al. In vivo quantification of myocardial amyloid deposits in patients with suspected transthyretin-related amyloidosis (ATTR). J Clin Med. 2020; 9(11), doi: 10.3390/jcm9113446, indexed in Pubmed: 33120935.
49. Dorbala S, Park MA, Cuddy S, et al. Absolute quantitation of cardiac ^{99m}Tc-pyrophosphate using cadmium-zinc-telluride-based SPECT/CT. J Nucl Med. 2021; 62(5): 716–722, doi: 10.2967/jnumed.120.247312, indexed in Pubmed: 32887756.